Selective Etching of Magnetic Tunnel Junction Materials Using CO/NH_3 Gas Mixture in Radio Frequency Pulse-Biased Inductively Coupled Plasmas

2013 Jpn. J. Appl. Phys. 52 05EB03

(http://iopscience.iop.org/1347-4065/52/5S2/05EB03)

Japanese Journal of Applied Physics **52** (2013) 05EB03 **REGULAR PAPER**
http://dx.doi.org/**10.7567/JJAP.52.05EB03**

Selective Etching of Magnetic Tunnel Junction Materials Using CO/NH_3 Gas Mixture in Radio Frequency Pulse-Biased Inductively Coupled Plasmas

Min Hwan Jeon[1], Hoe Jun Kim[2], Kyung Che Yang[2], Se Koo Kang[1], Kyong Nam Kim[2], and Geun Young Yeom[1,2*]

[1]*SKKU Advanced Institute of Nano Technology (SAINT), Sungkyunkwan University, Suwon, Gyeonggi 440-746, Republic of Korea*
[2]*Department of Materials Science and Engineering, Sungkyunkwan University, Suwon, Gyeonggi 440-746, Republic Korea*
E-mail: gyyeom@skku.edu

Received December 4, 2012; accepted February 26, 2013; published online May 20, 2013

The etch characteristics of magnetic tunneling junction (MTJ) materials and the etch selectivity over W have been investigated using RF pulse-biased conditions in addition to the continuous wave (CW) bias condition with a CO/NH_3 gas combination in an inductively coupled plasma system. By using a time-averaged substrate DC bias voltage condition for the RF pulse biasing, the etch rates of MTJ materials for the RF pulse-biased conditions were generally similar to those etched using the CW RF bias condition even though the etch rates were slightly decreased with decreasing the duty percentage of the RF pulse biasing. However, the use of the RF pulse biasing improved the etch selectivity of the MTJ materials over mask materials such as W. When the surface roughness and the residual thickness remaining on the etched surface of the MTJ material such as CoFeB were investigated by using atomic force microscopy (AFM) and X-ray photoelectron spectroscopy (XPS), respectively, it was clear that the use of the RF pulse biasing instead of CW RF biasing also decreased the residual thickness and the surface roughness. This is believed to be related to the formation of a more uniform chemically reacted layer on the etch CoFeB surface during the RF pulse-biased etching condition.

1. Introduction

Recently, magnetic random access memory (MRAM) has made prominent progress in memory performance and has brought a bright future for the next-generation nonvolatile memory owing to its faster access time, higher storage density, lower operating voltage, and infinite rewrite time as compared with conventional RAM devices.[1–4] In particular, spin transfer torque (STT)-MRAM has been investigated extensively owing to the possibility in an attempt to overcome the scaling limit of MRAM devices.[5–10]

The multilayer of the magnetic tunnel junction (MTJ) is the most important material in the structure of the MRAM device, which typically consists of CoFeB/MgO/CoFeB.[11] For the mass storage in addition to high-capacity nonvolatile MRAM devices, the dry etch process of this multilayer MTJ material is one of the most important processes owing to the difficulty in the formation of volatile compounds between ferromagnetic materials and etch gases, and therefore, the difficulty in the etching of MTJ materials. The MTJ materials have been generally etched by physical sputtering using Ar^+ ion beam etchers or Ar^+ plasma etching,[12,13] but this has several disadvantages such as etch damage, sidewall redeposition of the sputter-etched residue, low etch selectivity, and low etch anisotropy. The MTJ materials have also been etched using conventional reactive ion etchers such as inductively coupled plasma (ICP) etchers with halogen gases, such as Cl_2 and BCl_3 at room temperature.[14,15] However, recently, owing to the corrosion of the etched MTJ material surface and the low etch selectivity over mask materials, the etching of MTJ materials using noncorrosive gases such as CO/NH_3, CH_3OH, and CH_4 has been investigated by many research groups.[16–25] When noncorrosive gases are used in the etching of MTJ materials, owing to the low vapor pressures of compounds formed between the MTJ materials and the noncorrosive etching gases, the problems such as low etch rates of MTJ materials, and low etch selectivity over mask materials, low etch anisotropy still remain even though the problems related to halogen gases such as corrosion can be eliminated.

To enhance the volatility of etch products and to increase the etch rates of MTJ materials, other techniques such as substrate heating and source power RF pulsing have been also investigated.[26–28] The study on the effect of substrate temperature during the etching of the MTJ materials using CH_3OH in an ICP showed that, with the increase of substrate temperature from 20 to 120 °C, the deposition of sidewall residue was decreased while the etch rates of MTJ materials were increased. In the case of etching the MTJ materials using the pulsing of microwave plasma in Cl_2-based gases (source power pulsing not bias power pulsing), high etch rates of MTJ materials without corrosion or delamination were observed, while corrosion and delamination of MTJ materials were observed in the etching using continuous wave (CW) microwave plasmas. The researchers believe that the negative ions formed during the power-off period enhance the chemical reactions on the surface of magnetic films. They reported that the magnetic characteristics were also significantly improved by using the source power-pulsed plasma because of reduced residues in addition to the improvement of the etch profile.[29]

Even though it was reported that the source power pulsing improved the MTJ etch characteristics, it is believed that the bias power pulsing instead of the source power pulsing can also improve the etch characteristics of MTJ materials. In this study, an RF pulse-biasing technique has been applied in the etching of MTJ materials, such as CoFeB and MgO, and W has been used as one of the hard mask materials and its effect on the etch characteristics was investigated in an ICP system using a CO/NH_3 gas mixture, which has been investigated to show high etch rates in previous studies.[30]

2. Experimental Methods

In this study, the MRAM-related materials were etched by various RF pulse-bias conditions using a CO/NH_3 gas combination in an ICP system. The ICP etch system with 8 in. diameter (STS PLC) was used in this experiment. A schematic diagram of the ICP etch system is shown in Fig. 1. As shown in this figure, a one-turn inductive coil was wound around the ceramic chamber wall and a 13.56 MHz

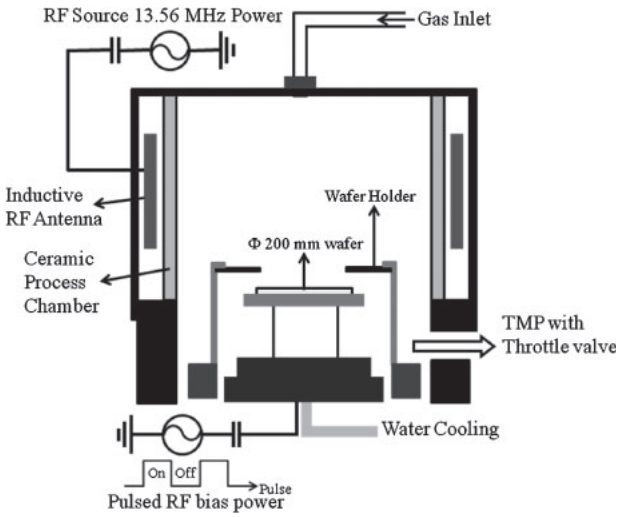

Fig. 1. Schematic diagram of the ICP etching system used in this study.

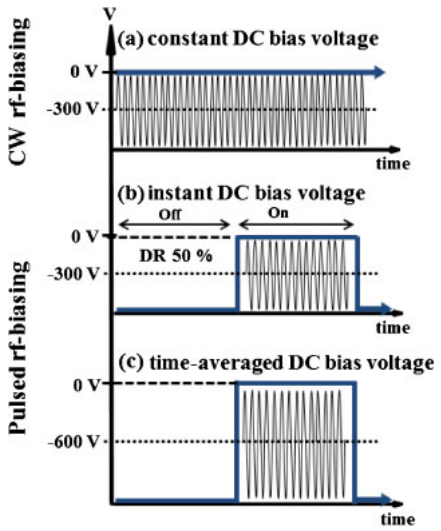

Fig. 2. (Color online) (a) CW RF biasing at −300 V of constant DC bias voltage condition. (b) and (c) show the rf pulsed biasing with the 50% duty ratio at −300 V of DC bias voltage condition for instant DC biasing and time-averaged DC biasing, respectively.

RF power was applied to the inductive coil. Also, a 13.56 MHz RF power as RF-biasing was applied to the substrate and it was cooled to about 20–30 °C using water cooling. To apply the RF pulsed power, a pulse/function generator (HP 8116A), a signal generator (HP 8657B) and an RF power amplifier (ENI A1000) were installed to the substrate.

As MRAM materials, the MTJ-related materials, such as CoFeB and MgO, and W used as the hard mask material were used to compare the etch characteristics. The MTJ-related materials and the hard mask material were prepared using a co-sputter deposition technique. These materials were etched using a CO/NH_3 gas combination for effective chemical reactions, and the gas flow rates of CO and NH_3 were fixed at 12.5 and 37.5 sccm, respectively. The source power of 500 W and DC bias voltage of −300 V were used to etch the MRAM-related materials. For the RF pulsed biasing, the RF power applied to the substrate was turned on and off at the frequency of 50 kHz with different duty percentages varied from 100 to 30%. During the pulsed biasing, the DC bias voltage was maintained at −300 V (both with an instant DC bias voltage condition and with a time-averaged DC bias voltage condition: for the time-averaged DC bias voltage condition of −300 V, the instant DC bias voltage during the pulse-on time was higher than −300 V and increased with decreasing the duty percentage to compensate the no-bias voltage time during the pulse-off period). Figure 2(a) shows the CW RF biasing at −300 V of constant DC bias voltage condition and Figs. 2(b) and 2(c) show the RF pulsed biasing with the 50% duty percentage at −300 V of DC bias voltage condition for instant DC biasing and time-averaged DC biasing, respectively. As shown, in the case of the time-averaged DC bias voltage condition of −300 V, the DC bias voltage was increased to about −600 V to have the time-averaged voltage of −300 V. The process pressure and the total flow rate were fixed at 5 mTorr and 50 sccm, respectively.

After the etching of the MTJ-related materials and the hard mask material, a step profilometer (Tencor Alpha step 500) was used to measure the etch depth. Among the investigated MTJ-related materials, the surface morphology of the etched CoFeB was analyzed with a high-resolution atomic force microscopy (HRAFM; SPA-300HV) system and the chemical bonding characteristics of the CoFeB film after the etching were also investigated by X-ray photoelectron spectroscopy (XPS; VG Microtech ESCA2000) using a Mg Kα twin-anode source.

3. Results and Discussion

The etch rates of the materials such as CoFeB, MgO, and W and the etch selectivities of CoFeB and MgO over W were investigated as a function of pulse duty percentage at a fixed DC bias voltage of −300 V (for both instant DC bias voltage and time-averaged DC bias voltage), and the results are shown in Fig. 3(a) for the etch rates and Fig. 3(b) for the etch selectivities. The pulse frequency was kept at 50 kHz. The ICP power, the process pressure of CO (12.5 sccm)/NH_3 (37.5 sccm), and the substrate temperature were also maintained at 500 W, 5 mTorr, and 20–30 °C, respectively. As shown in Fig. 3(a), for the instant DC bias voltage condition, the etch rates of MgO and CoFeB were decreased from 10.5 (MgO)/12 (CoFeB) nm/min to about 4 nm/min (for both MgO and CoFeB) with the decrease of the pulse duty percentage from 100 (CW) to 30%. The MTJ materials were also etched with the time-averaged DC bias voltage condition and, as also shown in Fig. 3(a), the etch rates of MgO and CoFeB were decreased only slightly from 10 (MgO)–12 (CoFeB) to 8 (MgO)–9 (CoFeB) nm/min with decreasing the pulse duty percentage from 100 to 30%. The etch rates were not significantly decreased for the time-averaged constant DC bias voltage condition because the instant DC bias voltage during the pulse-on time increased with decreasing pulse duty percentage to have an average −300 V of DC bias voltage by showing about −415, −585, and −920 V for the pulse duty percentages of 70, 50, and 30%, respectively. The significant decrease of etch rate with the decrease of pulse duty percentage for the instant DC bias voltage condition is due to the decreased etch time during the one etch pulse cycle by maintaining the constant DC bias voltage during pulse-on time only. By using the time-

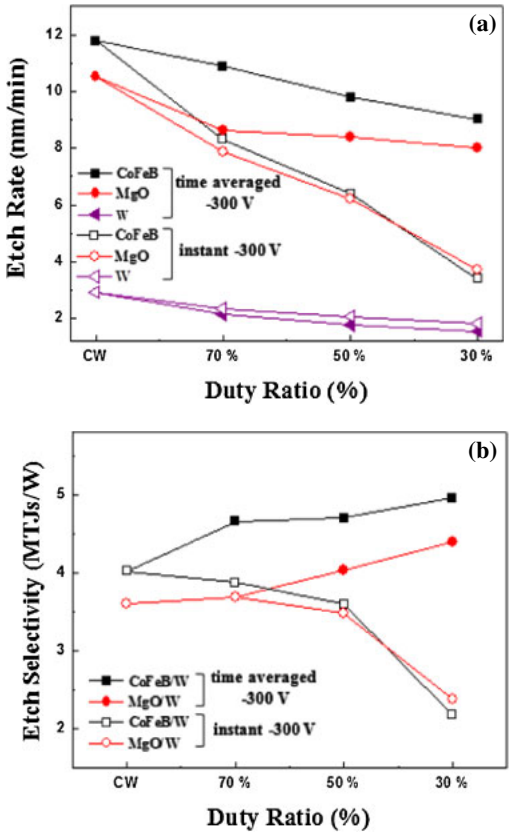

Fig. 3. (Color online) Etch characteristics of MTJ-related materials and W as a function of pulse duty percentage at a fixed DC bias voltage of −300 V. (a) Etch rates of MTJ materials and W and (b) etch selectivities of MTJ materials over W. The pulse frequency was kept at 50 kHz. The ICP power, the process pressure of CO (12.5 sccm)/NH_3 (37.5 sccm), and the substrate temperature were also maintained at 500 W, 5 mTorr, and 20–30 °C, respectively. As the constant DC bias voltage during the pulsing, the instant DC bias voltage condition and the time-averaged DC bias voltage condition were used.

averaged constant DC bias voltage condition, due to the increased ion bombardment energy with the decrease of the duty percentage, the etch rates of MTJ materials were not significantly decreased even though the ion bombardment time during the one etch pulse cycle is decreased with the decrease of pulse duty percentage. The slight decrease of etch rates of MTJ materials with decreasing pulse duty percentage for the time-averaged constant DC bias voltage condition is possibly related to the nonlinear relationship of etch rate or sputter yield with DC bias voltage.[31)]

When the etch selectivities were measured, as shown in Fig. 3(b), for the instant DC bias voltage condition, the etch selectivities of MgO and CoFeB over W were decreased from 3.5 (MgO)–4 (CoFeB) to 2.1–2.2 (for both MgO and CoFeB) with decreasing the duty percentage from 100 to 30%, as shown in Fig. 3(b). However, for the time-averaged DC bias voltage condition, the etch selectivities of MgO and CoFeB over W were increased from 3.5 (MgO)–4 (CoFeB) to 4.5 (MgO)–5 (CoFeB) with decreasing the duty percentage from 100 to 30%. During the pulse-off time, the MTJ surface reacts with CO molecules such as CO, CO^*, and CO^+ in the plasma and could form more stable and volatile metal compounds with increasing the pulse-off time. Table I shows the vapor pressure of the carbonyl compounds for Co, Fe, and W.[32–34)] No carbonyl compound for Mg was

Table I. Vapor pressures of the carbonyl compounds for Co, Fe, and W. No carbonyl compound for Mg was reported.

	Vapor pressure or melting and boiling points	Reference
Co	$Co_2(CO)_8$: 3.2×10^{-3} kPa at 288 K $\log P(\text{kPa}) = 12.79 - 4402/T$	32
Fe	$Fe(CO)_5$: 1.97 kPa at 288 K $\log P(\text{mmHg}) = 8.45 - 2096.7/T$	32, 33
B	B_2H_6 Melting point: 108.15 K B_2H_6 Boiling point: 180.4 K	34
W	$W(CO)_6$: 9.7×10^{-4} kPa at 288 K $\log P(\text{kPa}) = 10.66 - 3886/T$	32

reported. As shown in Table I, the vapor pressure of the carbonyl compounds is the highest for $Fe(CO)_5$ and the vapor pressure of $Co_2(CO)_8$ is also higher than that of $W(CO)_6$ at the same temperature of 288°K. Therefore, the improved etch selectivity of CoFeB over W with the decreasing the pulse duty percentage for the time-averaged DC bias voltage condition could be partially related to the differences in the vapor pressure of the metal formed on the etched CoFeB surface, which might be related to metal carbonyl compounds. However, the decrease of etch selectivity at the instant DC bias voltage condition with the decrease of pulse duty percentage appears to suggest that the stable carbonyl compounds shown in Table I may not be easily formed at room temperature even for the pulsed plasma etching. In fact, it is also known that, for MTJ-related metals, owing to the extremely large size of these metal carbonyl molecules, due to the thermodynamically unfavorable processes in the formation of these metal carbonyls by the recombination of metals with CO gas and the low dissociation energies of the metal carbonyls the metal carbonyls cannot be easily formed during the conventional etching condition. Therefore, similarly in our etching condition, the stoichiometric and volatile metal carbonyl compounds shown in Table I may not be formed. Instead, nonstoichiometric metal compounds, which are less volatile than the stoichiometric metal carbonyl compounds in Table I but more volatile than metal itself or metal oxide, might be formed during the etching. These nonstoichiometric metal compounds need ion bombardment or sputtering for enhanced etching. By increasing the ion bombardment energy, the metal compounds formed during the CoFeB etching could show a higher etch rate than the W compound and the etch selectivities appeared to be increased with the decrease of pulse duty percentage for the time-averaged DC bias voltage condition.

The thickness and species of the chemically reacted layer formed on the etched CoFeB surfaces as a function of the pulse duty percentage were investigated using XPS. Figure 4 shows the XPS narrow scan data of Co 2p, Fe 2p, and B 1s during the depth profiling of the CoFeB surface etched with CW and 30% pulse duty percentage. The samples were etched for 3 min in CO/NH_3 with the time-averaged DC bias voltage condition of −300 V and the other etch conditions were the same as those in Fig. 3. The etched CoFeB was sputter-etched in the XPS chamber by an Ar^+ ion gun at 2 μA of ion current and 3 kV of ion energy for the depth

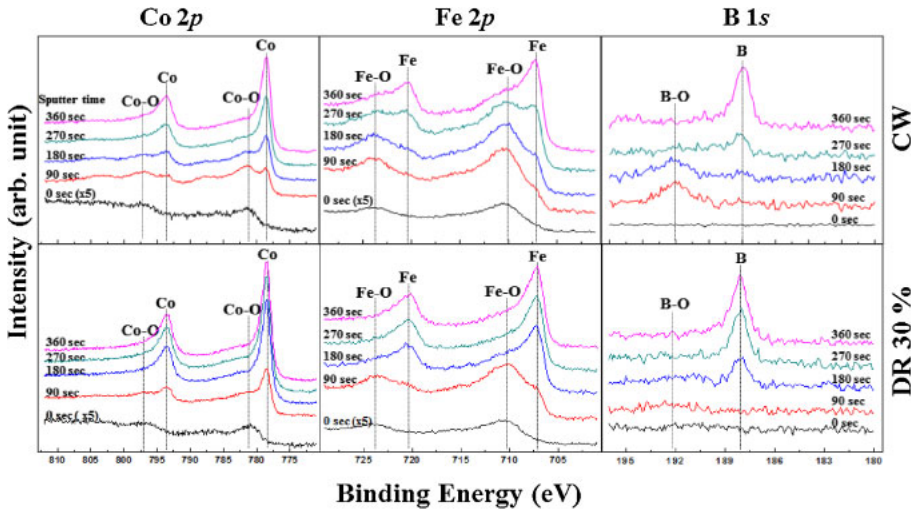

Fig. 4. (Color online) XPS narrow scan data of Co 2p, Fe 2p, and B 1s during the depth profiling of the CoFeB surface etched with CW and 30% pulse duty percentage. The samples were etched for 3 min with the time-averaged DC bias voltage condition of −300 V and the other etch conditions are the same as those in Fig. 3.

profiling. The surfaces were measured every 90 s of Ar^+ ion sputter etching for 360 s. When the CoFeB surface was measured before the etching, the pure metal binding energies were observed at 778.3 and 793.2 eV for Co 2p, 707 and 720.2 eV for Fe 2p, and 188 eV for B 1s. For the etched CoFeB, in addition to the pure metal peaks, additional peaks were observed at 781 and 797.1 eV for Co 2p, 710 and 723.5 eV for Fe 2p, and 192 eV for B 1s. The additional peaks were located at energies higher than those of pure metal peaks indicating the formation of metal compounds such as metal oxides. However, owing to the lack of information on the location of the metal carbonyl-related bonding peak, the formation of any metal carbonyl-related bonding could not be identified even though the etched CoFeB surface is rich in carbon and oxygen (shown in Fig. 5). After 90 s of sputter etching by Ar^+ ions, no carbon was detected on the etched CoFeB surface, and the observed additional peaks appear to be related to the formation of metal oxides such as $Co(OH)_x$ or Co_xO_y, Fe_xO_y, and B_xO_y. The peak binding energies were the same for the CoFeB surfaces etched by both 100% (CW) and 30% pulse duty percentage. However, the XPS peaks related to the pure metals of Co, Fe, and B emerged at the smaller Ar^+ ion sputter etch time for the CoFeB sample etched with 30% of pulse duty percentage indicating a smaller thickness of the chemically reacted layer than the CoFeB etched with CW rf biasing.

Figure 5 shows the relative atomic percentages of the etched CoFeB surface measured by XPS depth profiling as a function of Ar^+ ion sputter etch time for the CoFeB samples etched for various pulse duty percentages including the CoFeB etched with the CW biasing. The etch conditions are the same as those in Fig. 4. Before etching of the CoFeB, the relative atomic percentage of Co : Fe : B was 51 : 36 : 13%. As shown in the figure, initially, the surfaces of the etched CoFeB samples were rich in carbon and oxygen. After the Ar^+ ion sputtering for 90 s, all the carbon was removed, indicating a very thin carbon-related layer on the etched CoFeB surfaces, and oxygen-rich metal oxide layers were exposed. Further Ar^+ ion sputter etching showed that the oxygen percentage on the etched CoFeB surfaces decreased while the percentages of Co, Fe, and B increased with the increase of Ar^+ ion sputter etch time, that is, at a deeper location from the CoFeB surface. After the 360 s of sputter etching, the metallic surfaces appear to emerge for most of the samples except for CoFeB etched with 100% (CW). Comparing the CoFeB samples etched for different pulse duty percentages of (a) 100% (CW), (b) 70%, (c) 50%, and (d) 30%, the CoFeB etched with a smaller pulse duty percentage showed a lower Ar^+ ion sputter etch time for the recovery of metallic CoFeB percentages indicating a thinner chemically reacted layer on the etched CoFeB surface.

The surface roughness of the CoFeB samples etched with various pulse duty percentages was investigated using AFM and the results are shown in Fig. 6. The etch conditions were the same as those in Fig. 5. The surface roughness of the CoFeB before etching was included for reference. As shown in Fig. 5, the surface roughness of the CoFeB before etching was 0.81 nm, however, after the etching, the surface roughness was increased for all of the etched CoFeB samples. However, the surface roughness was decreased with the decrease of pulse duty percentage, showing about 4.46 nm for 100% (CW), 2.95 nm for 70%, 2.68 nm for 50%, and 2.27 nm for 30% pulse duty percentage; therefore, a lower surface roughness was obtained at a smaller duty percentage.

The thinner chemically reacted layer and the smoother etched surface for the smaller pulse duty cycle observed in Figs. 5 and 6, respectively, appear to be related to the formation of more metal compounds on the surface during the pulse-off time and the more uniform sputter removal of the compounds with a higher ion energy. Figure 7 shows a schematic drawing of one of the possible reaction mechanisms during the etching using CW rf biasing (100% pulse duty percentage) and 50% pulsed duty percentage with the time-averaged DC bias voltage condition. During the etching of CoFeB using the CW rf biasing, a chemically reacted layer could be formed on a different area of the CoFeB surface while the surface is continuously etched by reactive ions. That is, owing to the differences in CoFeB surface

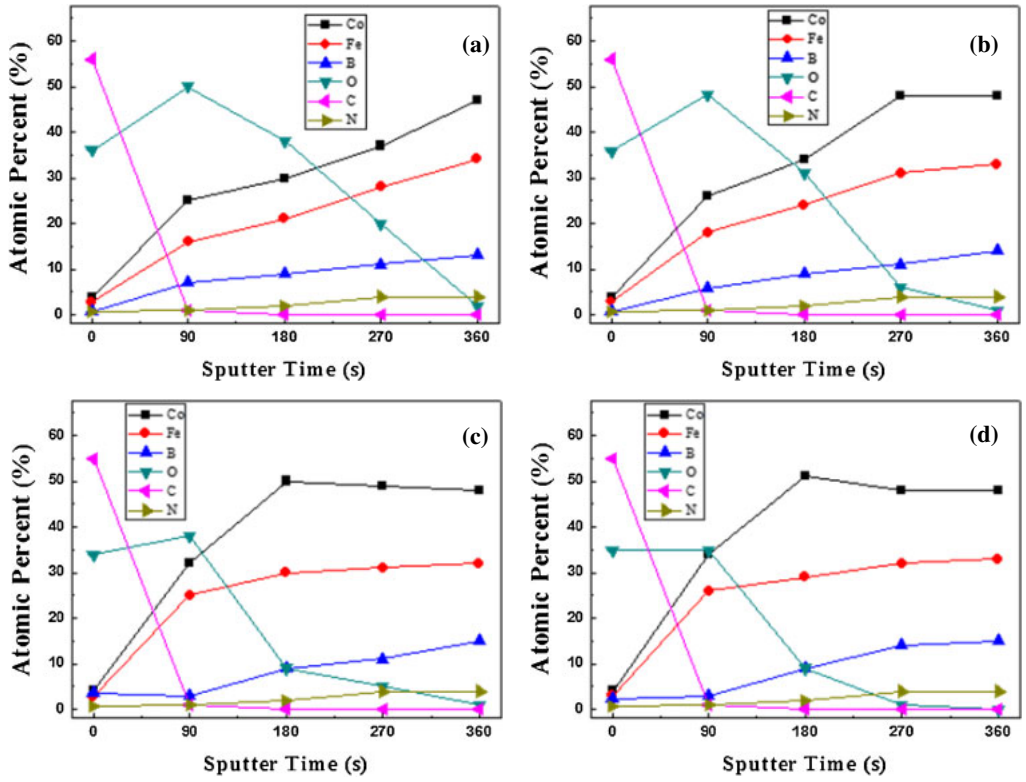

Fig. 5. (Color online) Relative atomic percentages of the etched CoFeB surface measured by XPS depth profiling as a function of Ar^+ ion sputter etch time for the CoFeB samples etched for various pulse duty percentages including the CoFeB etched with the CW biasing. (a) CW, (b) DR 70%, (c) DR 50%, and (d) DR 30%. The etch conditions are the same as those in Fig. 4.

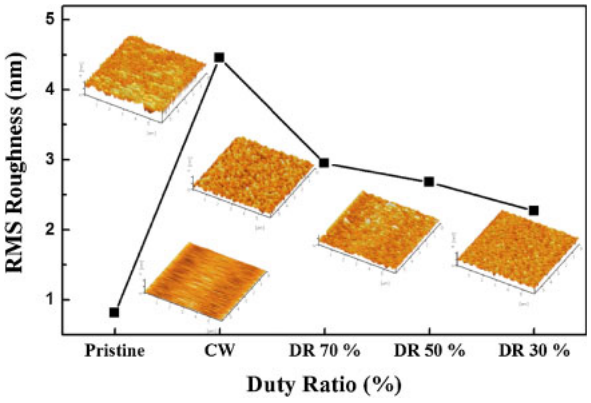

Fig. 6. (Color online) AFM surface roughness of the etched CoFeB as a function of pulse duty percentage using a CO/NH_3 gas combination in the ICP system. The etch conditions are the same as those in Fig. 4.

characteristics such as grain boundary, defects, and local compositional difference, the chemically reacted surface layers can be formed locally not uniformly on the surface and the local chemically reacted layer may be etched more selectively than the local layer with the metal/metal oxide by the low energy ion bombardment during the etching with CW rf biasing. This could increase not only the surface roughness but also the thickness of the remaining chemically reacted layer, as shown in Figs. 5 and 6. However, when the CoFeB is etched using the pulsed DC biasing with the constant time-averaged DC bias voltage condition, during the pulse-off time, the chemically reacted layer is formed more uniformly on the surface due to the nonexistence of ion bombardment and this layer could be etched nonselectively by the higher ion energy bombardment during the pulse-on time. Therefore, it is believed that the combination of a uniform chemically reacted layer on the CoFeB surface during the pulse-off time and the nonselective etching of the chemically reacted layer during the pulse-on time appears to exhibit a thinner chemically reacted residual layer and smoother CoFeB surface for the pulsed biasing with the constant time-averaged DC bias voltage condition.

4. Conclusions

MRAM-related materials such as CoFeB, MgO, and W were etched using rf pulse-biased conditions using an ICP system with a CO/NH_3 gas combination and the etch characteristics of MRAM-related materials and the surface characteristics of the etched CoFeB were investigated as a function of pulse duty percentage from 100 (CW biasing) to 30%. By using the time-averaged constant DC voltage condition for the pulsed biasing, which increases the instant DC bias voltage with decreasing the pulse duty percentage, the etch selectivity of MTJ materials over W could be improved without significantly decreasing the etch rates of MTJ materials. The improved etch selectivity of MTJ materials over W by using the pulsed biasing is believed to be related to the higher ion energy bombardment during the pulse-on time and the formation of a chemically reacted layer during the pulse-off time. In addition, by using the pulsed biasing, with the decrease of pulse duty percentage, not only the surface roughness but also the thickness of the chemically reacted layer was decreased, which appears to be related to the formation of a more uniform chemically reacted layer on

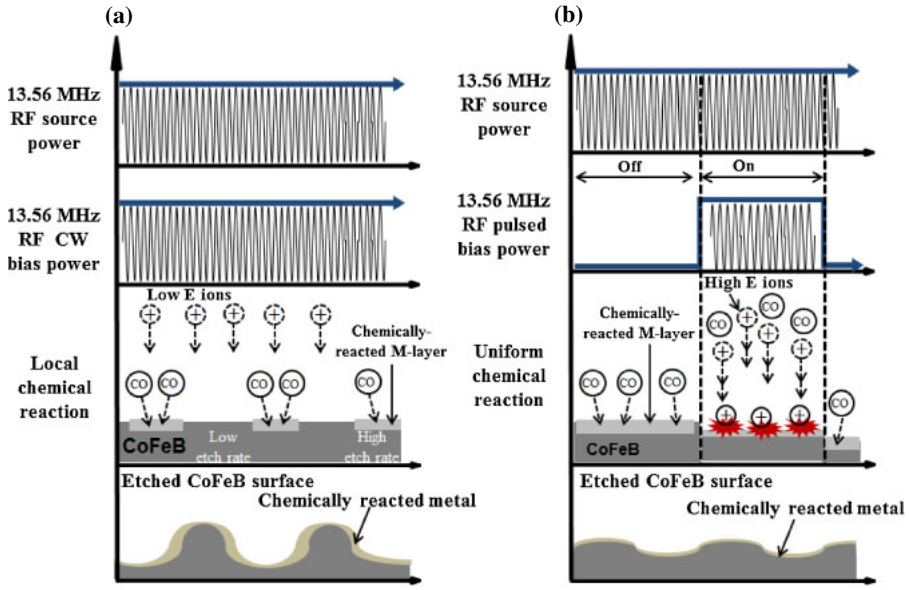

Fig. 7. (Color online) Schematic drawing of one of the possible reaction mechanisms during the etching using CW biasing (100% pulse duty cycle) and 50% pulsed duty cycle.

the CoFeB surface during the pulse-off time and the more nonselective etching of the layer during the pulse-on time. Using the 30% pulse duty percentage (50 kHz), −300 V of time-averaged constant DC bias voltage, 500 W of 13.56 MHz ICP power, and 5 mTorr of CO/NH_3 (12.5 sccm:37.5 sccm), CoFeB and MgO could be etched with ~9 and ~8 nm/min with the etch selectivities over W of 5 and 4.5, respectively, at room temperature.

Acknowledgments

This work was supported by the SRC project No. 2011-IN-2219. The authors would like to thank Dr. Satyarth Suri and Dr. Bob Turkot in Intel Corporation for helpful discussion on MRAM etching. This work was partially supported by the Industrial Strategic Technology Development Program (10041681, Development of fundamental technology for 10 nm process semiconductor and 10 G size large area process with high plasma density and VHF condition) funded by the Ministry of Knowledge Economy (MKE, Korea) and the World Class University program of the National Research Foundation of Korea (Grant No. R32-10124).

1) Y. Otani, H. Kubota, A. Fukushima, H. Maehara, T. Osada, S. Yuasa, and K. Ando: IEEE Trans. Magn. **43** (2007) 2776.
2) G. Muller, T. Happ, M. Kund, G. Y. Lee, N. Nagel, and R. Sezi: IEDM Tech. Dig., 2004, p. 567.
3) T. M. Maffitt, J. K. DeBrosse, J. A. Gabric, E. T. Gow, M. C. Lamorey, J. S. Parenteau, D. R. Willmott, M. A. Wood, and W. J. Gallagher: IBM J. Res. Dev. **50** (2006) 25.
4) K. Kim and G. H. Koh: Proc. 24th Int. Conf. Microelectronics, 2004, p. 377.
5) H. Kubota, A. Fukushima, Y. Otani, S. Yuasa, K. Ando, H. Maehara, K. Tsunekawa, D. D. Djayaprawira, N. Watanabe, and Y. Suzuki: Jpn. J. Appl. Phys. **44** (2005) L1237.
6) M. Hosomi, H. Yamagishi, T. Yamamoto, K. Bessho, Y. Higo, K. Yamane, H. Yamada, M. Shoji, H. Hachino, C. Fukumoto, H. Nagao, and H. Kano: IEDM Tech. Dig., 2005, p. 459.
7) J. Hayakawa, S. Ikeda, Y. M. Lee, R. Sasaki, T. Meguro, F. Matsukura, H. Takahashi, and H. Ohno: IEEE Trans. Magn. **44** (2008) 1962.
8) Y. Huai, D. Apalkov, Z. Diao, Y. Ding, A. Panchula, M. Pakala, L. Wang, and E. Chen: Jpn. J. Appl. Phys. **45** (2006) 3835.
9) S. Mangin, D. Ravelosona, J. A. Katine, M. J. Carey, B. D. Terris, and E. E. Fullerton: Nat. Mater. **5** (2006) 210.
10) S. Ikeda, K. Miura, H. Yamamoto, K. Mizunuma, H. D. Gan, M. Endo, S. Kanai, J. Hayakawa, F. Matsukura, and H. Ohno: Nat. Mater. **9** (2010) 721.
11) D. D. Djayaprawira, K. Tsunekawa, M. Nagai, H. Maehara, S. Yamagata, N. Watanabe, S. Yuasa, and K. Ando: Appl. Phys. Lett. **86** (2005) 092502.
12) K. Sugiura, S. Takahashi, M. Amano, T. Kajiyama, M. Iwayama, Y. Asao, N. Shimomura, T. Kishi, S. Ikegawa, H. Yoda, and A. Nitayama: Jpn. J. Appl. Phys. **48** (2009) 08HD02.
13) K. Kinoshita, H. Utsumi, K. Suemitsu, H. Hada, and T. Sugibayashi: Jpn. J. Appl. Phys. **49** (2010) 08JB02.
14) K. Ichihara and M. Hara: Jpn. J. Appl. Phys. **36** (1997) 4874.
15) K. B. Jung, E. S. Lambers, J. R. Childress, S. J. Pearton, M. Jenson, and A. T. Hurst: Appl. Phys. Lett. **71** (1997) 1255.
16) I. Nakatani: IEEE Trans. Magn. **32** (1996) 4448.
17) T. Osada, M. Doi, K. Sakamoto, H. Maehara, and Y. Kodaira: Proc. 26th Int. Symp. Dry Process (DPS), 2004, p. 127.
18) X. Peng, S. Wakeham, A. Morrone, A. Axdal, M. Feldbaum, J. Hwu, T. Boonstra, Y. Chen, and J. Ding: Vacuum **83** (2009) 1007.
19) K. B. Jung, J. Hong, H. Cho, S. Onishi, D. Johnson, Y. D. Park, J. R. Childress, and S. J. Pearton: J. Electrochem. Soc. **146** (1999) 2163.
20) N. Matsui, K. Mashimo, A. Egami, A. Konishi, O. Okada, and T. Tsukada: Vacuum **66** (2002) 479.
21) H. Kubota, K. Ueda, Y. Ando, and T. Miyazaki: J. Magn. Magn. Mater. **272–276** (2004) E1421.
22) A. S. Orland and R. Blumenthal: J. Vac. Sci. Technol. B **23** (2005) 1597.
23) X. Kong, D. Krasa, H. P. Zhou, W. Williams, S. McVitie, J. M. R. Weaver, and C. D. W. Wilkinson: Microelectron. Eng. **85** (2008) 988.
24) K. Kinoshita, T. Yamamoto, H. Honjo, N. Kasai, S. Ikeda, and H. Ohno: Jpn. J. Appl. Phys. **51** (2012) 08HA01.
25) K. B. Jung, J. Hong, H. Cho, S. Onishi, D. Johnson, Y. D. Park, J. R. Childress, and S. J. Pearton: J. Vac. Sci. Technol. A **17** (1999) 535.
26) M. S. Lee and W. J. Lee: Appl. Surf. Sci. **258** (2012) 8100.
27) T. Mukai, H. Hada, S. Tahara, H. Yoda, and S. Samukawa: Jpn. J. Appl. Phys. **45** (2006) 5542.
28) T. Mukai, B. Jinnai, Y. Fukumoto, N. Ohshima, H. Hada, and S. Samukawa: J. Appl. Phys. **102** (2007) 073303.
29) T. Mukai, N. Ohshima, H. Hada, and S. Samukawa: J. Vac. Sci. Technol. A **25** (2007) 432.
30) J. Y. Park, S.-K. Kang, M. H. Jeon, M. S. Jhon, and G. Y. Yeom: J. Electrochem. Soc. **158** (2011) H1.
31) K. Karahashi, T. Ito, and S. Hamaguchi: Proc. 33rd. Int. Symp. Dry Process (DPS), 2011, A-6, p. 11.
32) M. L. Garner, D. Chandra, and K. H. Lau: J. Phase Equilibria **16** (1995) 24.
33) A. G. Gilbert and K. G. P. Sulzmann: J. Electrochem. Soc. **121** (1974) 832.
34) D. R. Lide: *Handbook of Chemistry and Physics* (CRC Press, Boca Raton, FL, 2004) 84th ed, p. 5-7.